Static magnetic response of multi-core particles

Alexey O. Ivanov*
Ural Mathematical Center, Institute of Nature Sciences and Mathematics, Ural Federal University, 51 Lenin Avenue, 620000, Russia

Frank Ludwig
Institute for Electrical Measurement Science and Fundamental Electrical Engineering, and Laboratory for Emerging Nanometrology (LENA), TU Braunschweig, D-38106 Braunschweig, Germany

(Dated: August 22, 2020)

We present theoretical calculations of the characteristics of the static magnetic response of multi-core magnetic nanoparticles. These particles contain a considerable number ($\sim 10^2$) of single-domain magnetic nanocrystallites, which are modelled as uniformly magnetized balls with uniaxial magneto-crystalline anisotropy, the energetic barrier of which is comparable with the thermal energy. Thus, we model a multi-core magnetic nanoparticle as an ensemble of superparamagnetic nanoparticles, the position and the easy magnetization axis of which are fixed, but randomly distributed. Summing up the magnetic moments of the nanocrystallites inside a multi-core particle, we thus obtain the magnetic moment of the multi-core particle under the assumption that magnetic interactions between the nanocrystallites can be neglected. It is found that the weak-field magnetic response of these multi-core particles is independent of anisotropy constant. The model is compared with recent experimental data and good agreement is found.

I. INTRODUCTION

A magnetic multi-core particle (MCP) [1] has a two-scale structure. On the "large" scale (typical order ~ 100 nm), being suspended in some liquid carrier, MCPs are involved in intensive Brownian motion, and in the suspension they play a part of single structural units, having some effective physical and chemical characteristics. But on the "small" scale (~ 10 nm) it contains a rather large number of magnetic cores (nanosized single-domain magnetic crystallites), "glued" by a polymer or other nonmagnetic material. The typical size of MCPs is between the size of particles in standard ferrofluids and in magnetorheological suspensions. So, their physical properties occupy an intermediate position between the properties of these systems. In part, the multi-core-based ferrofluids are more sedimentary stable than the standard magnetorheological suspensions with micron-sized particles. At the same time, they demonstrate much stronger magnetorheological effects [2–4] than standard ferrofluids with single-core nanosized particles. The combination of the stability with the high response to an applied field has large potential for many applications, what causes the growing interest within the last decade [5–9]. The potential efficiency of MCPs for the magnetic hyperthermia method of cancer therapy [1, 7, 8, 10–14] and magnetic particle imaging [15–17] has been demonstrated. A very detailed overview of particle synthesis, including the description of clustered magnetic particles and MCPs with almost regular spherical shape, can be found in a recent publication [1].

Being suspended in a liquid, the MCP system exhibits various structural transitions and self-assembly [18–22]. But focusing on possible applications, which are based on the response of MCPs to applied magnetic fields, the principal question is the determination of the magnetic moment of a single MCP and the magnetic properties of MCP suspensions. Known experimental observations [5, 6, 23, 24] and investigations by means of computer simulations [25–29] reveal a strong dependence of the "large" scale MCP magnetic properties on the "small" scale magnetic anisotropy of single-domain particles. To the best of our knowledge, no simple expressions were obtained, applicable for experimental estimations.

In the present paper we are going to trace the dependence of MCPs magnetic response to the magnetic properties of single-domain particles. For this purpose, in Section II we first define the model of single MCP in II A, paying attention to various definitions of the MCP magnetic moment in II B. Section III is devoted to the development of theoretical approaches, starting from the "small" scale of a single nanoparticle (III A) and going up to the "large" scale of MCP magnetic moment calculation (III B). Importantly, we use here the approach of non-interacting cores since their positions inside the MCP body are fixed, and the core magnetic moments are rather small due to small sizes of crystallites. But we are aware of the fact that magnetic interactions should be included if the cores are very densely packed. The main feature of the "small" scale is the uni-axial magnetic anisotropy of the core magnetic material; and we develop our model for arbitrary values of magnetic anisotropy energy. The magnetic properties of the MCP suspension are discussed theoretically (III C) with account for interparticle magnetic interactions. We suggest here the approximation for each MCP as an uniformly magnetized sphere; this

* Alexey.Ivanov@urfu.ru

simplification allows us to use the dipole-dipole interparticle potential [30]. All obtained theoretical expressions are demonstrated in Section IV with plots for different values of magnetic anisotropy. In addition, comparing it with experimental data [24], we show the efficiency of the developed model in predicting MCPs effective magnetic characteristics. We end with our Conclusion.

II. MODEL

A. Model of the multi-core particle

Let us consider a spherical multi-core particle (MCP) of volume V_p, made from some hard (non-elastic) and absolutely non-magnetic material (for example, silica). The typical MCPs diameter is of the order of hundred nanometers ($\sim$ 100 nm). Some number N of spherical single-domain superparamagnetic nanoparticles (SNP) is embedded in the MCP body; we consider an uni-axial magneto-crystalline structure of the SNP material. The MCP structure is illustrated in Fig. 1(a). The magnetic core diameter d_m of SNP is assumed as $10-20$ nm, so their number N varies from several dozens to several hundreds, depending on SNP volume concentration φ. Each SNP has a magnetic core volume $v_m = \pi d_m^3/6$, and its magnetic material is characterized by the bulk saturation magnetization M_0 and the magnetic anisotropy constant K. So, the absolute value of the SNP magnetic moment is given by $m = M_0 v_m$. The center position of each i-th SNP ($i \in [1; N]$) is defined by its radius-vector $\mathbf{q}_i$, and the direction of the SNP easy magnetization axis is determined by the unit vector $\hat{\mathbf{n}}_i$. Both the positions of SNPs and the directions of their easy magnetization axes are distributed uniformly; so the arrays $\{\mathbf{q}_i\}$ and $\{\hat{\mathbf{n}}_i\}$ contain the random set of SNPs positions/orientations inside a MCP under the condition of non overlapping SNPs. Finally, we restrict our analysis to the case of small SNP volume fractions, $\varphi < 0.1$.

The last restriction allows us to neglect the inter-core magnetic interaction. At first sight, this approximation looks very crude. But our argumentation is the following. The SNP positions are fixed inside the hard MCP body, so the SNP cannot move and cannot form the liquid-like correlated nearest-neighbor order, induced by the interparticle interaction. The mean inter-core magnetic energy may be estimated as $\mu_0 m^2 \varphi / 4\pi d_m^3$, where μ_0 is the vacuum magnetic permeability. For example, for typical magnetite SNPs the parameters are the following: the bulk magnetization amounts to $M_0 \approx 480$ kA/m at room temperature; the magnetic core diameter is $d_m \approx 15$ nm; the SNP volume fraction is $\varphi = 0.1$. So we get a typical value for the magnetic energy as $\sim 2 \cdot 10^{-21}$J, which is a factor of two smaller than the room temperature thermal energy $k_B T \sim 4 \cdot 10^{-21}$ J. So, the deviation in magnetic response of the SNP ensemble from ideal non-interacting behavior is rather small and can be ignored for low SNP number densities.

For common nanosized particles, as considered before, the anisotropy barrier $K v_m$ may be comparable to the thermal energy, and so thermal fluctuations result in stochastic reorientations of the magnetic moment inside SNP. The mean value of the SNP magnetic moment, measured over a long time, will be equal to zero. This behaviour is known as Néel superparamagnetism, and it is a characteristic of nanosized particles only [31]. Superparamagnetic fluctuations are commonly described as the thermally activated rotations of the magnetic moment inside the SNP. Importantly, this mechanism means that even if particle positions and orientations (easy axes) are frozen, the magnetic moments are still able to rotate, subject to the potential energy U_N, and the magnetic energy U_m of the interaction with the field:

$$U_N(i) = -K v_m \left(\hat{\mathbf{m}}_i \cdot \hat{\mathbf{n}}_i\right)^2 \ , \tag{1}$$

$$U_m(i) = -\mu_0 \left(\mathbf{m}_i \cdot \mathbf{H}\right) = -\mu_0 m H \left(\hat{\mathbf{m}}_i \cdot \hat{\mathbf{h}}\right) \ . \tag{2}$$

Here $\hat{\mathbf{m}} = \mathbf{m}/m$ is the unit vector, the applied magnetic field $\mathbf{H}$ has strength H and orientation $\hat{\mathbf{h}} = \mathbf{H}/H$. Two dimensionless parameters are associated with these terms, which measure the corresponding energies with respect to the thermal energy $k_B T$,

$$\sigma = \frac{K v_m}{k_B T} \ , \quad \alpha = \frac{\mu_0 m H}{k_B T} \ , \tag{3}$$

σ is the anisotropy parameter, and α is the Langevin parameter characterizing the particle-field interactions.

B. Magnetic moment of MCP

Let us define the laboratory coordinate system, and the applied magnetic field $\hat{\mathbf{h}} = (0, 0, 1)$ is in Oz direction. The orientation (easy axis) of the i-th SNP is the unit vector $\hat{\mathbf{n}}_i = (\sin\xi_i \cos\psi_i, \sin\xi_i \sin\psi_i, \cos\xi_i)$, where ξ_i and ψ_i are, respectively, the polar and azimuthal angles in the laboratory frame. The i-th SNP magnetic moment is $\mathbf{m}_i = m\hat{\mathbf{m}}_i$, where $\hat{\mathbf{m}}_i = (\sin\omega_i \cos\zeta_i, \sin\omega_i \sin\zeta_i, \cos\omega_i)$, and ω_i and ζ_i are, respectively, the polar and azimuthal angles in the body-fixed frame of the particle. These vectors are shown in Fig. 1(b).

Concerning the meaning of the MCP magnetic moment $\boldsymbol{\mu}$, it is worth mentioning that there is some controversy in its definition. Correctly, the vector $\boldsymbol{\mu}$ is defined as the vector sum of all SNPs magnetic moments, and this summation must be done at some fixed time moment:

$$\boldsymbol{\mu}_\mathrm{s} \equiv \sum_{i=1}^{N} \mathbf{m}_i \ . \tag{4}$$

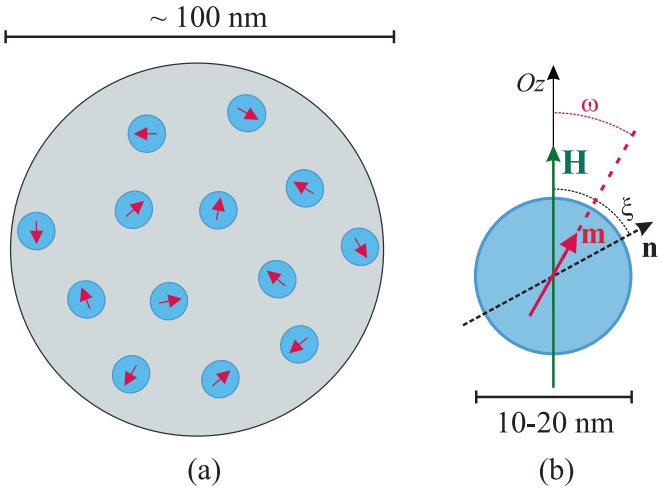

FIG. 1. (a) Model of a multi-core particle (MCP). The single-domain superparamagnetic particles (SNP) are randomly (uniformly) distributed and oriented in MCP non-magnetic body. (b) The orientation of the SNP is given by the body-fixed, magnetic easy axis vector $\hat{\mathbf{n}}$. The orientation of the particle magnetic moment $\mathbf{m}$ can be different from the easy-axis vector due to superparamagnetic fluctuations. The angles ω and ξ are also shown.

But due to superparamagnetic fluctuations in $\mathbf{m}_i$ this definition represents an instantaneous snapshot; so we term it $\boldsymbol{\mu}_{\rm s}$. A more accurate definition takes into account these fluctuations on the level of time averaging:

$$\boldsymbol{\mu}_{\rm t} \equiv \left\langle \sum_{i=1}^{N} \mathbf{m}_i \right\rangle_t , \quad \langle ... \rangle_t \equiv \lim_{t\to\infty} \frac{1}{t} \int_0^t ...dt \ . \qquad (5)$$

Here the angle brackets stand for the time averaging over a rather long time period t, exceeding the time scale of experimental measurements. Obviously, both definitions (4) and (5) give zero MCP magnetic moment in the absence of an external magnetic field; of course, this conclusion holds true for expression (4) only for rather large number N.

Another definition of MCP magnetic moment was used, for example, in Refs. [5, 6], where the mean-squared value was called the effective MCP magnetic moment:

$$\mu_{\rm eff} \equiv \left\langle \left(\sum_{i=1}^{N} \mathbf{m}_i \right)^2 \right\rangle_t^{1/2} . \qquad (6)$$

Clearly, for the case of zero external magnetic field this approach results in non-zero effective MNP magnetic moment, which appears to be proportional to $\sqrt{N}$. However, this $\mu_{\rm eff}$ is σ-independent. Evidently, an applied magnetic field increases $\mu_{\rm eff}$ [5], and this increase is described by a parabolic field dependence. Contrary, the Monte Carlo simulations [25, 27, 28] evidences that the MNP magnetic moment is dependent on magnetic anisotropy σ of the SNP material.

The mean-squared magnetic moment becomes uninformative when studying the magnetic response of a suspension of MCPs. It is very important here to trace for the direction of MCP magnetic moments, which could be calculated formally from expression (5). Assuming the statistical behavior of SNP system close to statistical ensemble, the time averaging in Eq. (5) could be replaced with the ensemble averaging:

$$\boldsymbol{\mu} \equiv m\hat{\mathbf{h}} \sum_{i=1}^{N} \int d\hat{\mathbf{m}}_i \left(\hat{\mathbf{m}}_i \cdot \hat{\mathbf{h}} \right) W_i \left(\hat{\mathbf{m}}_i, \hat{\mathbf{n}}_i \right) , \qquad (7)$$

$$\int d\hat{\mathbf{m}}_i = \frac{1}{4\pi} \int_0^{2\pi} d\zeta_i \int_{-1}^{1} d\cos\omega_i \ . \qquad (8)$$

Here we use the fact that the non-zero component of each SNP magnetic moment is induced by an external field along its direction, so that $\boldsymbol{\mu} || \hat{\mathbf{h}}$; this fact results in the appearance of the scalar product $\left(\hat{\mathbf{m}}_i \cdot \hat{\mathbf{h}} \right)$. Of course, we should average over all possible orientations of the i-th magnetic moment, so that $\int d\hat{\mathbf{m}}_i \cdot 1 = 1$. The weight function W_i has the meaning of the one-particle probability density for the i-th magnetic moment to be oriented in some direction. Summation over i in (7) should be made over the given random array $\{\hat{\mathbf{n}}_i\}$ of SNPs easy axes.

For non-interacting SNP the orientation probability density is well-known, for example, [31]:

$$W_i \left(\hat{\mathbf{m}}_i, \hat{\mathbf{n}}_i \right) = \frac{\exp\left[\sigma \left(\hat{\mathbf{m}}_i \cdot \hat{\mathbf{n}}_i \right)^2 + \alpha \left(\hat{\mathbf{m}}_i \cdot \hat{\mathbf{h}} \right) \right]}{Z_i \left(\hat{\mathbf{n}}_i \right)} , \qquad (9)$$

$$Z_i \left(\hat{\mathbf{n}}_i \right) = \int d\hat{\mathbf{m}}_i \exp\left[\sigma \left(\hat{\mathbf{m}}_i \cdot \hat{\mathbf{n}}_i \right)^2 + \alpha \left(\hat{\mathbf{m}}_i \cdot \hat{\mathbf{h}} \right) \right] , \qquad (10)$$

where Z_i stands for the normalization constant. In the zero-field limit this function demonstrates two peaks at $(\hat{\mathbf{m}}_i \cdot \hat{\mathbf{n}}_i) = \pm 1$

$$W_i \left(\hat{\mathbf{m}}_i, \hat{\mathbf{n}}_i \right) = R(\sigma)^{-1} \exp\left[\sigma \left(\hat{\mathbf{m}}_i \cdot \hat{\mathbf{n}}_i \right)^2 \right] , \qquad (11)$$

$$R(\sigma) = \int_0^1 \exp\left(\sigma t^2 \right) dt \ , \qquad (12)$$

the function $R(\sigma)$, independent of the easy axis direction $\hat{\mathbf{n}}_i$, was introduced first in Ref. [32].

In the limit of infinitely weak magnetic anisotropy ($\sigma = 0$) the expressions (7) and (9) give the Langevin magnetization, which is true for freely rotating magnetic moments without interparticle interaction:

$$\mu = m\sum_{i=1}^{N}\int d\hat{\mathbf{m}}_i \left(\hat{\mathbf{m}}_i\cdot\hat{\mathbf{h}}\right)\frac{\exp\left[\alpha\left(\hat{\mathbf{m}}_i\cdot\hat{\mathbf{h}}\right)\right]}{Z_i} \qquad (13)$$

$$= \frac{Nm}{2}\int_{-1}^{1} d\cos\omega_i \frac{\alpha\cos\omega_i\exp\left(\alpha\cos\omega_i\right)}{\sinh\alpha}$$

$$= Nm\left(\coth\alpha - \frac{1}{\alpha}\right) \equiv NmL(\alpha)\ , \quad \sigma = 0\ .$$

This case is very simple since W_i becomes $\hat{\mathbf{n}}_i$ independent; and the absolute value μ of the MCP magnetic moment is proportional to N.

III. THEORY

Importantly, the MCP magnetic moment should be calculated as a function of an external field strength α for arbitrary values of relative anisotropy energy σ. The essential point here is that the magnetic response of the MCP is dictated by the internal rotation of the magnetic moments of the SNPs.

A. Single SNP magnetic moment

Let us consider a randomly chosen SNP (number i); its easy axis is oriented at an angle ξ_i with respect to the magnetic field; see Fig. 1(b). In this case, $(\hat{\mathbf{m}}_i\cdot\hat{\mathbf{n}}_i) = \sin\xi_i\sin\omega_i\cos\left(\zeta_i-\psi_i\right) + \cos\xi_i\cos\omega_i$, and $\left(\hat{\mathbf{m}}_i\cdot\hat{\mathbf{h}}\right) = \cos\omega_i$. An important difference from the preceding case (13) is that the one-particle distribution function W_i becomes dependent on the angles ξ_i and ψ_i:

$$W_i(\omega_i,\zeta_i-\psi_i,\xi_i;\alpha,\sigma) = \frac{\exp\left(\alpha\cos\omega_i\right)}{Z_i(\xi_i;\alpha,\sigma)} \qquad (14)$$

$$\times\exp\left\{\sigma\left[\sin\xi_i\sin\omega_i\cos\left(\zeta_i-\psi_i\right)+\cos\xi_i\cos\omega_i\right]^2\right\}\ .$$

Here we emphasize that all angles are variables, but α and σ are parameters. But since the easy axes are frozen, only ω_i and ζ_i are thermal degrees of freedom here, over which the normalization coefficient Z_i is averaged. So, Z_i turns out to be only ξ_i-dependent and can be presented in the following way [31, 33]:

$$Z_i(\xi_i;\alpha,\sigma) = \frac{1}{2}\int_{-1}^{1}\exp\left(\sigma t^2+\alpha t\cos\xi_i\right) \qquad (15)$$

$$\times I_0\left(\alpha\sin\xi_i\sqrt{1-t^2}\right)dt\ ,$$

with the special cases $Z_i(\xi_i;\alpha,0) = \alpha^{-1}\sinh\alpha$, and $Z_i(\xi_i;0,\sigma) = R(\sigma)$; here $I_0(z)$ is the modified Bessel function of zero order. At large values of α and σ the function Z_i grows exponentially; but from an application point of view the region of weak-to-moderate parameters is of major interest. Using Taylor series over small $\alpha<1$ with the accuracy of α^4, we expand the integrand in terms of Legendre polynomials $P_k(z)$:

$$\exp\left(\alpha t\cos\xi_i\right)I_0\left(\alpha\sin\xi_i\sqrt{1-t^2}\right) \qquad (16)$$

$$= 1+\frac{\alpha^2}{6}\left[1+2P_2(t)P_2(\cos\xi_i)\right]$$

$$+\frac{\alpha^4}{120}\left[1+\frac{20}{7}P_2(t)P_2(\cos\xi_i)+\frac{8}{7}P_4(t)P_4(\cos\xi_i)\right]\ .$$

Due to integration in (15), only even terms in α are important here. Introducing this expansion, at a weak magnetic field ($\alpha<1$), expression (15) transforms into

$$Z_i(\xi_i;\alpha,\sigma) = R(\sigma)\left[1+\frac{\alpha^2}{6}A_\xi(\xi_i;\sigma)\right. \qquad (17)$$

$$\left.+\frac{\alpha^4}{120}B_\xi(\xi_i;\sigma)\right]+O\left(\alpha^6\right)\ ,$$

$$A_\xi(\xi_i;\sigma) = 1+\frac{2P_2(\cos\xi_i)}{R(\sigma)}\int_0^1\exp\left(\sigma t^2\right)P_2(t)\ dt$$

$$= 1+\left[A_{||}(\sigma)-1\right]P_2(\cos\xi_i)\ ,$$

$$A_{||}(\sigma) = 3\frac{d\ln R(\sigma)}{d\sigma} = \frac{3}{2\sigma}\left[\frac{\exp(\sigma)}{R(\sigma)}-1\right]\ ,$$

$$B_\xi(\xi_i;\sigma) = 1+\frac{20P_2(\cos\xi_i)}{7R(\sigma)}\int_0^1\exp\left(\sigma t^2\right)P_2(t)\ dt$$

$$+\frac{8P_4(\cos\xi_i)}{7R(\sigma)}\int_0^1\exp\left(\sigma t^2\right)P_4(t)\ dt\ .$$

Here, functions $A_{||}$ and A_ξ were introduced in Refs. [31, 34]; they describe the initial magnetic susceptibility of immobilized SNPs, the easy axes of which are directed parallel to the field ($A_{||}$) and tilted at some angle ξ (A_ξ). For magnetically soft SNP, $A_{||}(0)=1$; and it increases monotonously with growing σ

$$A_{||}(\sigma)\approx 1+\frac{4\sigma}{15}+\frac{8\sigma^2}{315}-\frac{16\sigma^3}{4725}-\frac{32\sigma^4}{31185}\ , \quad \sigma<3\ , \qquad (18)$$

reaching asymptotically the value $A_{||}(\sigma \to \infty) \to 3$:

$$A_{||}(\sigma) \approx 3\left(1 - \frac{1}{\sigma} - \frac{1}{2\sigma^2}\right) \ , \quad \sigma > 3 \ . \tag{19}$$

It is interesting that there is a magic angle $\xi_0 = \arccos(1/\sqrt{3})$, at which the coefficient $A_\xi(\xi_0;\sigma) = 1$ and it is hence independent of σ.

The magnetic moment of each i-th SNP contributes to the magnetic moment of the MCP with its Oz component m_{iz}:

$$m_{iz}(\xi_i;\alpha,\sigma) = m\ \frac{\partial \ln Z_i(\xi_i;\alpha,\sigma)}{\partial\alpha} \ . \tag{20}$$

Evidently, $m_{iz}(\xi_i;0,\sigma) = 0$ for $\forall\xi_i \in [0;\pi]$ and $\forall\sigma \in [0;\infty)$. The functional dependencies of m_{iz} on parameters ξ_i, α, σ can be obtained only numerically since the integral in (15) could not be calculated in explicit functions.

For the case of a weak applied field within the accuracy of expansion (17) we get from expression (20)

$$\mathbf{m}_i(\xi_i;\alpha<1,\sigma) = \frac{\mu_0 m^2}{3k_BT}\mathbf{H} \tag{21}$$

$$\times\left\{A_\xi(\xi_i;\sigma) + \frac{\alpha^2}{10}\left[B_\xi(\xi_i;\sigma) - \frac{5}{3}A_\xi(\xi_i;\sigma)^2\right]\right\} \ .$$

So, the magnetic moment of each SNP, embedded into the MCP body, is directed along an external field and is induced by this external field.

In addition, for hard magnetic nanoparticles ($\sigma \gg 1$) the expression (20) can be converted to a simpler form [28, 31, 33], which is valid in the limit $\sigma \to \infty$:

$$m_{iz}(\xi_i;\alpha,\sigma\to\infty) = m\cos\xi_i \tanh(\alpha\cos\xi_i) \ . \tag{22}$$

B. MCP magnetic moment

The next step is to sum up all SNP magnetic moments m_{iz} in definition (7) over the array of their easy axes directions $\{\hat{\mathbf{n}}_i\}$. Of course, for each given MCP this summation can be done only numerically since the array of easy axes directions is unique. But talking about the effective magnetic moment of some randomly chosen averaged MCP it is acceptable to change the summation in expression (7) to continuous integration over the variable $\hat{\mathbf{n}}_i$:

$$\boldsymbol{\mu} \equiv \frac{N\hat{\mathbf{h}}}{2}\int_{-1}^{1} m_{iz}(\xi_i;\alpha,\sigma)\ d\cos\xi_i \tag{23}$$

$$= \frac{mN\hat{\mathbf{h}}}{2}\frac{\partial}{\partial\alpha}\int_{-1}^{1}\ln Z_i(\xi_i;\alpha,\sigma)\ d\cos\xi_i \ .$$

An interesting and very important effect follows from the weak-field asymptotic (21): the single MCP weak-field magnetic moment becomes σ independent after averaging over the random distribution of SNP easy axes:

$$\lim_{H\to 0}\frac{\mu}{H} \equiv \chi_{MCP}(0) = \frac{\mu_0 N m^2}{3k_BT} \tag{24}$$

$$\times\frac{1}{2}\int_{-1}^{1} A_\xi(\xi_i;\sigma)\ d\cos\xi_i = \frac{\mu_0 N m^2}{3k_BT}$$

The point is that the MCP static initial susceptibility $\chi_{MCP}(0)$ does not explicitly depend on the magnetic anisotropy constant K, since the last expression is σ-independent. This unexpected feature is a result of averaging (24) over the random distribution of immobilized SNP easy axes.

It is worth mentioning that the magnetic susceptibility is often measured with AC field magnetometers [23, 24], and the static value is associated with the zero-frequency limit of the real part of measured AC susceptibility. Here, the static susceptibility becomes dependent on the amplitude of the applied AC magnetic field [24]. The equilibrium analogy for this zero-frequency susceptibility is the ratio

$$\chi_{MCP}(H) = \mu(H)/H \ , \tag{25}$$

which we call the single MCP static field-dependent magnetic susceptibility. It is the measurable characteristic of both single MCP and suspension of MCPs. But, unfortunately, no simple expression for this function $\chi_{MCP}(H)$ could be obtained even within the simplification of non-interacting SNPs inside the single MCP. For the case of arbitrary-strength external magnetic field this function can be presented only with the help of numerical calculations of expressions (25), (23) and (15).

The weak-field behavior of the MCP magnetic susceptibility (25) follows from expression (21):

$$\chi_{MCP}(\alpha,\sigma) = \chi_{MCP}(0)\left[1 - \frac{\alpha^2}{15}D(\sigma)\right] \ , \tag{26}$$

$$D(\sigma) = 1 + \frac{1}{2}\left[A_{||}(\sigma) - 1\right]^2 \ .$$

So, this parabolic decrease is determined by the σ-dependent coefficient $D(\sigma)$, which is equal to unity for magnetically soft SNPs, $D(0) = 1$, and it increases monotonously with growing σ

$$D(\sigma) \approx 1 + \frac{8\sigma^2}{225} + \frac{32\sigma^3}{4725} - \frac{32\sigma^4}{55125} \ , \quad \sigma < 3 \ , \tag{27}$$

reaching asymptotically the value $D(\sigma \to \infty) \to 3$:

$$D(\sigma) \approx 3\left(1 - \frac{2}{\sigma} + \frac{1}{2\sigma^2}\right) , \quad \sigma > 3 . \tag{28}$$

C. Static magnetic response of MCP suspension

From the application point of view, the magnetic moment of MCP is important for predicting the magnetic properties of the suspension of MCPs. For this purpose we go to another scale of analysis, where each MCP becomes a new structural unit. The number density of MCPs is n, and we consider the sample with MCP suspension in a shape of a very long cylinder, the main axis of which is aligned along the Oz axis of the laboratory coordinate system. The static uniform magnetic field is also applied along this axis. The mentioned shape of the container allows us to avoid the demagnetizing effect and to assume an internal magnetic field into the sample being equal to an external field.

Neglecting first interparticle magnetic interactions, it is easy to obtain the magnetization law of the MCP suspension, since all MCPs are considered to be equal. It means that the absolute value of the Oz-directed vector of the suspension magnetization $\mathbf{M}_{\rm ni}$ of non-interacting MCPs is the sum of their magnetic moments, all of which are also aligned along this direction:

$$M_{\rm ni}(H) = n\mu(H) , \tag{29}$$

where the function $\mu(H)$ is given by equation (23). The static initial susceptibility $\chi_{\rm ni}$ of the suspension on non-interacting MCPs is evidently

$$\chi_{\rm ni} = \frac{\mu_0 n N m^2}{3k_B T} \equiv \chi_L , \tag{30}$$

and χ_L stands for the Langevin susceptibility of non-interacting particles. The product nN here has the meaning of the number of SNPs in a unit volume of the suspension. This equation can be interpreted in another way. From the "large" scale point of view, each MSP is considered as the structural unit with some effective characteristics, for example, with effective magnetic moment $\mu_{\rm eff}$. Thus, this expression (30) describes the initial magnetic susceptibility of the suspension of these non-interacting colloidal particles, the number density of which is n. Evidently, for this case the Langevin expression holds true, $\chi_{\rm ni} = \mu_0 n \mu_{\rm eff}^2 / 3k_B T$, and the mean squared effective magnetic moment $\mu_{\rm eff} = \sqrt{\mu_{\rm eff}^2}$ appears to be proportional to the square root of the SNP number N inside a single MCP, $\mu_{\rm eff} = \sqrt{N} m$; this result agrees with the conclusion of Refs. [5, 6].

Now we address an important question about the impact of interparticle magnetic interactions between MCP in the suspension. This point is very important because the MCP concentration may be rather large, and the MCPs are involved in Brownian motion; so they can move to a close contact and can be correlated through the interparticle magnetic interaction. Unfortunately, analytically this problem cannot be considered correctly due to the rather complicated internal structure of each MCP (see Fig. 1). The only simplification we should suggest here is the approximation of each MCP by a uniformly magnetized sphere with the same magnetic moment $\boldsymbol{\mu}$. This approximation is very important because we can use the dipole-dipole interaction potential for describing the interparticle magnetic interaction [30]. After that the problem should be solved on the simplest approach, known as the modified mean-field model of the 1-st order (MMF-1) [31, 35]. This approach, described in detail in Ref. [31], is based on the simple idea that the magnetic moment of each structural unit (i.e., a single MCP at this level of the theory) is influenced by an external magnetic field and by the summarized dipole-type magnetic field, produced by all other uniformly magnetized particles. So, this effective field $\mathbf{H}_{\rm e}(i)$, acting on the randomly chosen i-th MCP, can be expressed as follows:

$$\mathbf{H}_{\rm e}(i) = \mathbf{H} + \mathbf{H}_{\rm d}(i) , \tag{31}$$

$$\mathbf{H}_{\rm d}(i) = \frac{1}{4\pi} \sum_{j \neq i} \int \frac{d\mathbf{r}_j}{V} \frac{\boldsymbol{\mu}_j(H) \left[3\left(\hat{\mathbf{r}}_{ij} \cdot \hat{\mathbf{z}}\right)^2 - 1\right]}{|\mathbf{r}_i - \mathbf{r}_j|^3} \tag{32}$$

$$= \frac{\boldsymbol{M}_{\rm ni}(H)}{3} .$$

Here $\mathbf{r}_i$ and $\mathbf{r}_j$ are the radius-vectors of the centers of MCPs i and j; $\mathbf{r}_{ij} \equiv |\mathbf{r}_i - \mathbf{r}_j| = \hat{\mathbf{r}}_{ij} r_{ij}$, and $\hat{\mathbf{r}}_{ij}$ stands for the unit vector; $\hat{\mathbf{z}}$ is a unit vector along the Oz axis; the integral $\int d\mathbf{r}_j$ has the meaning of the averaging over all possible positions of j-th MCP in a sample volume V, excluding overlapping of particles. We also use here that the magnetic moments of all particles are directed along Oz axis. It should be pointed out that the integral over $\int d\mathbf{r}_j$ gives $4\pi/3$ for the case of a very long cylinder. It is worth mentioning that the MMF-1 approach appears to be very efficient not only for the description of static magnetic properties of ferrofluids, but also of dynamic susceptibility spectra [36, 37].

Inserting the effective field (31), (32) into the MCP magnetic moment (23), we get the resulting expressions for the suspension magnetization and the initial magnetic susceptibility:

$$M(H) = n\mu \left[H + \frac{n\mu(H)}{3}\right] \tag{33}$$

$$= \frac{nNm}{2} \int_{-1}^{1} \ln Z_i(\xi_i; \alpha_{\rm e}, \sigma) \; d\cos\xi_i ,$$

$$\alpha_{\rm e} = \alpha + \frac{\chi_L}{2}\int_{-1}^{1} \ln Z_j(\xi_j;\alpha,\sigma)\; d\cos\xi_j \;,$$

$$\chi = \chi_L\left(1+\frac{\chi_L}{3}\right) \;. \qquad (34)$$

Here $\alpha_{\rm e}$ stands for the effective value of the Langevin parameter; the second part of $\alpha_{\rm e}$ takes into account the magnetic interaction between MCPs; and the measure of this interaction is the Langevin susceptibility χ_L. An important feature is that the suspension initial susceptibility (34) is independent of the anisotropy parameter σ; and this expressions coincides with the prediction of the MMF-1 model for ferrofluids [31, 36]. The regions of MMF-1 validity are as follows [36, 37]: the static magnetic properties are well described at $\chi_L < 3$; the dynamic initial susceptibility spectra are well described at $\chi_L < 1$.

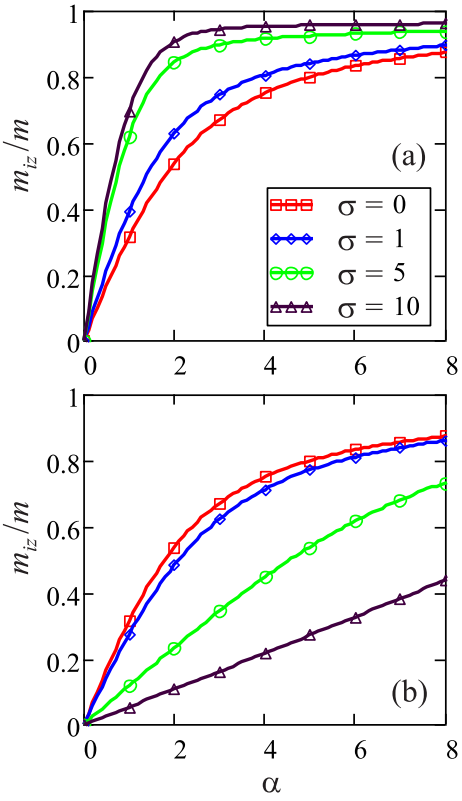

FIG. 2. The SNP relative magnetic moment m_{iz}/m (20) as a function of external field strength (in the Langevin units α) for different values of anisotropy parameter σ, given in the legend. The SNP easy magnetization axis is directed parallel (a) to the field, $\xi_i = 0$, and perpendicular (b) to the field, $\xi_i = \pi/2$. Calculated data are shown both as curves and symbols as indicated in the legend.

IV. RESULTS

First we show the Oz-component of a single SNP magnetic moment m_{iz}, calculated from expression (20) at various angles ξ_i between external field direction (Oz-axis) and the SNP easy magnetization axis. The field dependence of m_{iz}/m is shown in Fig. 2 for the case of parallel (Fig. 2(a)) and perpendicular (Fig. 2(b)) alignment. In case (a) we see a rapid growth of the induced SNP magnetic moment with a field strength; and the initial slope increases with σ. The last conclusion evidently follows from (21) and (17), since $A_\xi(\xi_i = 0;\sigma) = A_{||}(\sigma)$. So, the easy axes texturing in direction parallel to the field increases the magnetic response of a single SNP. The opposite effect we see in case of perpendicular alignment (b): the presence of a high anisotropy barrier inside a SNP leads to the suppression of the induced magnetic moment; clearly, $A_\xi(\xi_i = \pi/2;\sigma) = \left[3 - A_{||}(\sigma)\right]/2$ is a decreasing function of σ. The angle ξ_0 plays a part of the changeover angle between tendencies (a) and (b).

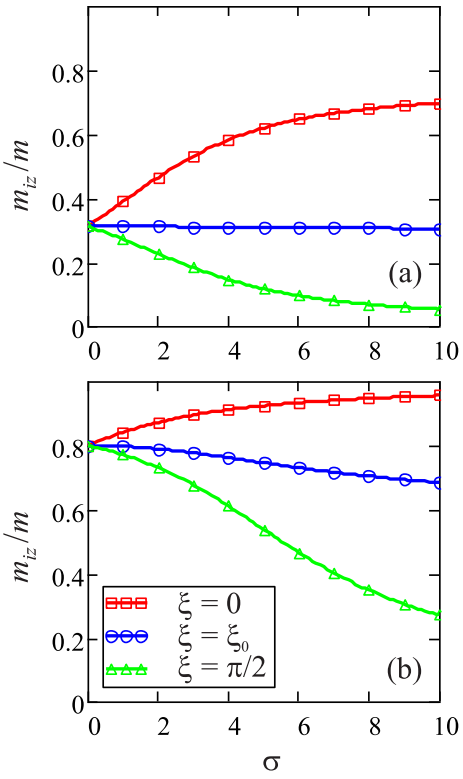

FIG. 3. The SNP relative magnetic moment m_{iz}/m (20) as a function of anisotropy parameter σ for different values of the angle ξ_i, given in the legend. An external file strength is $\alpha = 1$ (a) and 5 (b). Calculated data are shown both as curves and symbols as indicated in the legend.

The dependence of function m_{iz} on the anisotropy parameter σ is shown in Fig. 3 for three angles at two values of the Langevin parameter. The tendency is close to that shown in Fig. 2: for the changeover angle ξ_0 the SNP magnetic moment depends weakly on the SNP

magnetic anisotropy [middle curves in Fig. 3(a) and (b)]. For smaller angles, closer to parallel alignment, the SNP magnetic moment increases with σ, for larger angles ($\xi_0 \lesssim \xi \leq \pi/2$) the anisotropy barrier leads to a decrease of the SNP magnetic moment. Of course, there is a competition between the two energies: the particle - field energy measured with the Langevin parameter, and the anisotropy energy, measured in relative σ units. For the case 3(b) with $\alpha = 5$, the decrease becomes well expressed when σ becomes comparable with α.

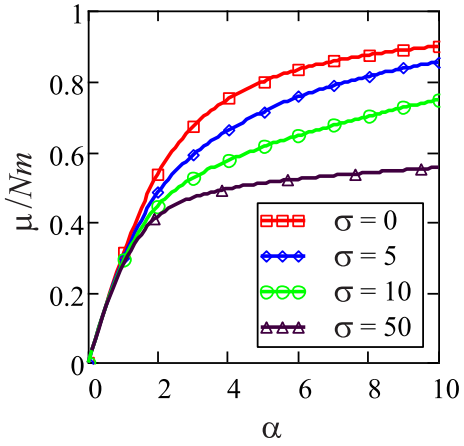

FIG. 4. The MCP relative magnetic moment μ/Nm (23) as a function of an external field strength (in the Langevin units α) for different values of anisotropy parameter σ, given in the legend. The easy axes of SNPs, embedded in MCP body, are distributed randomly. The red curve represents the Langevin function (13). Calculated data are shown both as curves and symbols as indicated in the legend.

Despite the different magnetic response of SNPs, oriented in various directions, the collective magnetic response of a SNP ensemble inside a single MCP demonstrates the classical type of magnetization curves after averaging over all possible orientations of SNP easy axes, Eq. (23). The field-induced MCP magnetic moment, presented in Fig. 4, shows the σ-dependent growth at moderate and strong external field. But, according to expression (24), the weak-field static magnetic response of a MCP appears to be independent of magnetic anisotropy. It should be pointed out that the last statement holds true only for rather large MCP, containing at least hundreds of SNP, the easy magnetization axes of which are randomly distributed in orientation space.

Turning back to the MCP magnetic susceptibility, we plot its calculated data (25) in Fig. 5 versus dimensionless magnetic field strength α for different values of the magnetic anisotropy parameter σ. The tendency is the same for each case: there is a plateau at small $\alpha < 0.1$ [see Fig. 5(b)], during which the susceptibility can be considered as constant; it is the region of validity of linear magnetostatics; at stronger fields the susceptibility monotonously decreases with the field amplitude. It should be pointed out that the parabolic asymptotic ex-

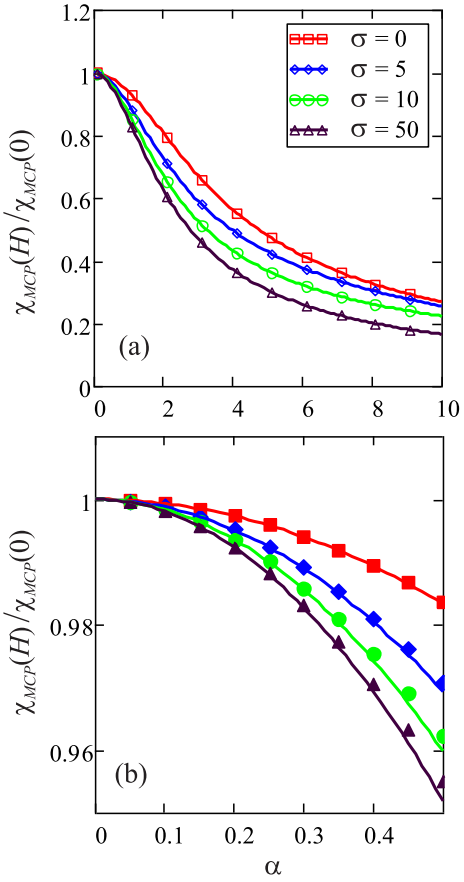

FIG. 5. The MCP magnetic susceptibility $\chi_{MCP}(H)/\chi_{MCP}(0)$ (25) as a function of external field strength (in the Langevin units α) for different values of anisotropy parameter σ, given in the legend for (a) and (b). The easy axes of SNPs, embedded in the MCP body, are distributed randomly. (a) Numerical solution of the equations (25) and (23) for a broad field range. Calculated data are shown both as curves and symbols as indicated in the legend. (b) The weak-field behavior, the numerical solutions of equations (25) and (23) are presented with filled symbols (the same as in the legend (a)), the solid lines show the parabolic decrease (26).

pression (26) describes very accurately the MCP magnetic susceptibility in the range of $\alpha < 0.5$, what makes it possible to use it for experimental data processing.

To demonstrate this, we use the experimental data from Ref. [24], where aqueous suspensions of two different iron oxide-based MCP systems were investigated. The BNF Starch particles (sample S1) from micromod Partikeltechnologie GmbH have a median particle size of 80 nm. The magnetite SNP average size is 20 nm determined from TEM images [24]. The second studied MCP system (sample S2) is FeraSpin XL from nanoPET Pharma GmbH. FeraSpin XL is a size fraction of FeraSpin R with a hydrodynamic diameter of about 60 nm. The core consists of a mixture of magnetite and maghemite with crystallite sizes of $5 - 8$ nm [24]. The AC susceptibility of both aqueous MCP suspensions were

measured using a custom-built AC susceptometer; the AC field amplitude can be varied from 0.2 mT to 9 mT with frequencies from 2 Hz to 9 kHz. The experimental data for zero-frequency field-dependent magnetic susceptibility are presented in Fig. 6 by filled symbols.

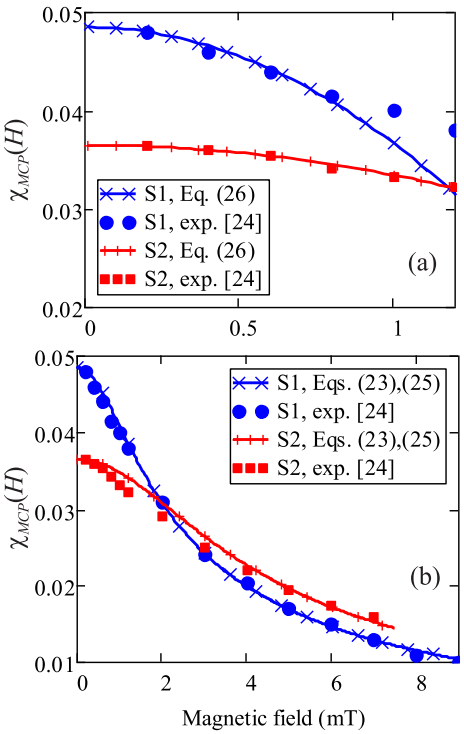

FIG. 6. Experimental data [24] for the field-dependent MCP magnetic susceptibility for samples S1 (BNF Starch) and S2 (FeraSpin XL), shown by filled symbols. Calculated data are shown both as curves and crosses as indicated in the legend. (a) The weak-field decrease is presented in comparison with the parabolic behavior (26) (curves). (b) Fit of the experimental data with equations (23) and (25) (curves) in the whole measured field range. The sample parameters, obtained from both fits (a) and (b), are given in Table I.

TABLE I. Estimated data for σ and μ for BNF Starch (S1) and FeraSpin XL (S2), obtained by fitting the experimental observations from Ref. [24].

	Fig. 6(a), (26)		Fig. 6(b), (23), (25)	
	σ	$\mu, 10^{-18}, \mathrm{Am}^2$	σ	$\mu, 10^{-18}, \mathrm{Am}^2$
BNF Starch	4	1.5	4	1.4
FeraSpin XL	1	1.1	1	0.9

First we fit the experimental data in the weak-field region with the help of the asymptotic expression (26); the comparison is shown in Fig. 6(a) and the obtained fitting results for σ and μ are shown in Table I. Both characteristic parameters turn out to be smaller for FeraSpin XL; this is consistent with the description of MCPs in both samples. In Fig. 6(b) we present the fit in the whole measured field range; here we use the numerical calculation of Eqs. (23) and (25), and the fitting results are also given in Table I. Of course, it is hard to expect that the present theoretical predictions coincide exactly with real experimental data since we did not consider the effect of polydispersity of real MCPs. The correct fit of the experimental data in the range of $4-9$ mT is accompanied by some deviations in the weak-field region; it is clearly seen for S2, for example, in Fig. 6(b). This result is expected since it is well-known [35] that the magnetic response of a nanoparticle ensemble is determined by the mean squared value of particle magnetic moment. Otherwise, in moderate and strong magnetic fields, the mean magnetic moment plays a major part. Of course, the last value is smaller than the first one for a polydisperse nanoparticle system. But we obtain the same tendency from fitting the experimental data; the estimated MCP magnetic moments appear to be smaller for both samples in the case when the fitting procedure is performed within the whole field range. Also, in our model we ignored the magnetic interaction between SNP inside a MCP, which might not be correct if the SNP are very densely packed (as e.g. in sample S2).

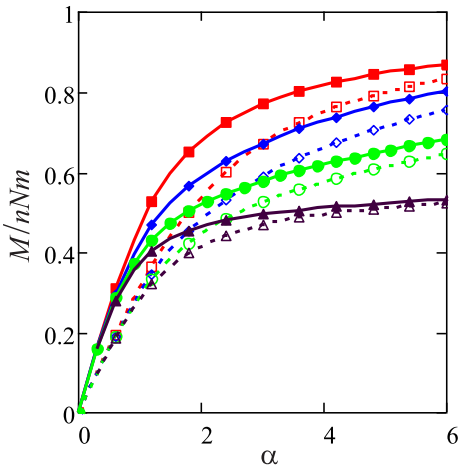

FIG. 7. Magnetization curve of the MCP suspension: the relative magnetization M/nNm [solid lines (33) with filled symbols] vs the magnetic field strength (measured in Langevin unit α). Dotted lines with open symbols show the magnetization for non-interacting MCPs (29). The values of anisotropy parameter are $\sigma = 0$ (squares, red); 5 (diamonds, blue); 10 (circles, green); 50 (triangles, brown), the same as in Figs. 4, 5. To demonstrate the contribution of interparticle magnetic interaction, we use here the Langevin susceptibility, $\chi_L = 2$.

The magnetization of a MCP suspension is shown in Fig. 7 for both the simplification of non-interacting MCPs (29) and the interacting MCPs (33) within the accuracy of the MMF-1 approach. Predictions of the present model are shown with dotted and solid curves for different values of the anisotropy parameter $\sigma = 0; 5; 10; 50$, the same as in Figs. 4, 5. It is clearly seen

that the initial slope of the $M(H)$ curves, that is the initial magnetic susceptibility, is independent of magnetic anisotropy. At the same time, for given values of anisotropy parameter σ and dimensionless magnetic field α, the interparticle interaction results in larger values of the suspension magnetization. Concerning the softness/hardness of the SNP magnetic material, the tendency is that the MCP suspension with magnetically hard SNP exhibits a smaller magnetization at a given magnetic field strength.

V. CONCLUSION

In this paper, we have presented theoretical calculations of the characteristics of the static magnetic response of multi-core magnetic particles. A distinctive feature of these particles is that they contain a considerable number ($\sim 10^2$) of nanosized inclusions, representing magnetic single-domain nanocrystallites. We model these "cores" as uniformly magnetized spheres with uni-axial magneto-crystalline anisotropy, the energetic barrier of which is comparable with the thermal energy. So, the nanocrystallite magnetic moment is not blocked, and thermal fluctuations result in the stochastic reorientation of the magnetic moment inside the crystallite. It means that we consider the model of a multi-core magnetic particle as an ensemble of superparamagnetic nanoparticles, the position and the easy magnetization axis of which are fixed in some random arrays. Here, the magnetic moments of a multi-core particles are induced by an external magnetic field. The essential point is that the magnetic response of a multi-core particle is dictated by the internal rotation of the magnetic moment within each nanocrystallite.

We calculate the field dependence of the crystallite magnetic moment for randomly given directions of the easy axis and arbitrary values of the magneto-crystalline energy barrier. Summing up the field-directed components of the SNP magnetic moments, we get the magnetic moment of the multi-core particles under the assumption that that magnetic intercrystallite interaction can be neglected. An important effect is observed here: the weak-field magnetic response of a multi-core particle turns out to be independent of the anisotropy energy due to random orientations of the core easy axes.

Our theoretical analysis results in simple expressions for the multi-core particle magnetic susceptibility, which can be effectively used for processing experimental data and estimating the magnetic characteristics of multi-core particles and their suspensions. The possibility of the prediction of these characteristics is of major importance for applications of these objects in bio-medicine and modern technologies.

ACKNOWLEDGMENTS

A. O. I. gratefully acknowledges research funding from the Ministry of Science and Higher Education of the Russian Federation (Contract No. 02.A03.21.006, Ural Mathematical Center project No. 075-02-2020-1537/1).

[1] V. Socoliuc, D. Peddis, V. I. Petrenko, M. V. Avdeev, D. Susan-Resiga, T. Szabó, R. Turcu, E. Tombácz, and L. Vékás, Magnetochemistry **6**, 2 (2020).
[2] D. Borin, A. Zubarev, D. Chirikov, R. Müller, and S. Odenbach, J. Magn. Magn. Mater. **323**, 1273 (2011).
[3] D. Y. Borin, A. Y. Zubarev, D. N. Chirikov, and S. Odenbach, J. Phys.: Cond. Matter **26**, 406002 (2014).
[4] M. Lopez-Lopez, D. Borin, and A. Zubarev, Phys. Rev. E **96**, 022605 (2017).
[5] V. Schaller, G. Wahnström, A. Sanz-Velasco, S. Gustafsson, E. Olsson, P. Enoksson, and C. Johansson, Phys. Rev. B **80**, 092406 (2009).
[6] F. Ahrentorp, A. Astalan, J. Blomgren, C. Jonasson, E. Wetterskog, P. Svedlindh, A. Lak, F. Ludwig, L. J. [van IJzendoorn], F. Westphal, C. Grüttner, N. Gehrke, S. Gustafsson, E. Olsson, and C. Johansson, J. Magn. Magn. Mater. **380**, 221 (2015).
[7] K. M. Krishnan, IEEE Transactions on Magnetics **46**, 2523 (2010).
[8] S. Dutz, M. Kettering, I. Hilger, R. Müller, and M. Zeisberger, Nanotechnology **22**, 265102 (2011).
[9] M. Lopez-Lopez, F. Nogueras-Lara, L. Rodriguez-Arco, N. Guigo, N. Sbirrazzuoli, A. Zubarev, S. Lacis, and P. Kuzhir, Phys. Rev. E **96**, 062604 (2017).
[10] C. Blanco-Andujar, D. Ortega, P. Southern, Q. A. Pankhurst, and N. T. K. Thanh, Nanoscale **7**, 1768 (2015).
[11] A. Zubarev, L. Iskakova, and A. Abu-Bakr, Physica A **467**, 59 (2017).
[12] A. Zubarev, Phys. Rev. E **98**, 032610 (2018).
[13] A. Zubarev, Phys. Rev. E **99**, 062609 (2019).
[14] M. Coïsson, G. Barrera, C. Appino, F. Celegato, L. Martino, A. Safronov, G. Kurlyandskaya, and P. Tiberto, J. Magn. Magn. Mater. **473**, 403 (2019).
[15] H. Arami, E. Teeman, A. Troksa, H. Bradshaw, K. Saatchi, A. Tomitaka, S. S. Gambhir, U. O. Häfeli, D. Liggitt, and K. M. Krishnan, Nanoscale **9**, 18723 (2017).
[16] G. Kurlyandskaya, S. Shcherbinin, S. Volchkov, S. Bhagat, E. Calle, R. Pérez, and M. Vazquez, J. Magn. Magn. Mater. **459**, 154 (2018).
[17] S. Ota, Y. Matsugi, T. Nakamura, R. Takeda, Y. Takemura, I. Kato, S. Nohara, T. Sasayama, T. Yoshida, and K. Enpuku, J. Magn. Magn. Mater. **474**, 311 (2019).
[18] E. S. Gonçalves, D. R. Cornejo, C. L. P. Oliveira, A. M. Figueiredo Neto, J. Depeyrot, F. A. Tourinho, and R. Aquino, Phys. Rev. E **91**, 042317 (2015).
[19] A. Zubarev, L. Iskakova, and M. Lopez-Lopez, Physica A **455**, 98 (2016).
[20] P. Ilg and A. Evangelopoulos, Phys. Rev. E **97**, 032610 (2018).
[21] J. Hernández-Rojas and F. Calvo, Phys. Rev. E **97**,

022601 (2018).
[22] G. Steinbach, M. Schreiber, D. Nissen, M. Albrecht, E. Novak, P. A. Sánchez, S. S. Kantorovich, S. Gemming, and A. Erbe, Phys. Rev. E **100**, 012608 (2019).
[23] J. Dieckhoff, D. Eberbeck, M. Schilling, and F. Ludwig, J. Appl. Phys. **119**, 043903 (2016).
[24] T. Kahmann and F. Ludwig, Journal of Applied Physics **127**, 233901 (2020).
[25] V. Schaller, G. Wahnström, A. Sanz-Velasco, P. Enoksson, and C. Johansson, J. Magn. Magn. Mater. **321**, 1400 (2009).
[26] A. Weddemann, A. Auge, D. Kappe, F. Wittbracht, and A. Hütten, J. Magn. Magn. Mater. **322**, 643 (2010).
[27] P. Ilg, Phys. Rev. B **95**, 214427 (2017).
[28] A. Kuznetsov, Phys. Rev. B **98**, 144418 (2018).
[29] P. Ilg, Phys. Rev. E **100**, 022608 (2019).
[30] B. F. Edwards, D. M. Riffe, J.-Y. Ji, and W. A. Booth, Am. J. Phys. **85**, 130 (2017).
[31] E. A. Elfimova, A. O. Ivanov, and P. J. Camp, Nanoscale **11**, 21834 (2019).
[32] Y. Raikher and M. Shliomis, J. Exp. Theor. Phys. **40**, 526 (1994).
[33] P. Cregg and L. Bessais, J. Magn. Magn. Mater. **202**, 554 (1999).
[34] A. O. Ivanov and E. A. Elfimova, Magnetohydrodynamics **55**, 59 (2019).
[35] A. O. Ivanov and O. B. Kuznetsova, Colloid J. **68**, 430 (2006).
[36] J. O. Sindt, P. J. Camp, S. S. Kantorovich, E. A. Elfimova, and A. O. Ivanov, Phys. Rev. E **93**, 063117 (2016).
[37] A. O. Ivanov and P. J. Camp, Phys. Rev. E **98**, 050602 (2018).